Supplementary Information for

Breaking the upper bound of siloxane uptake: Metal-Organic Frameworks as an adsorbent platform

Ezgi Gulcay [†a], **Paul Iacomi** [†a], **Kyung Ho Cho**[b], **Jong-San Chang**[b], **Guillaume Rioland**[c], **Sabine Devautour** [a], **and Guillaume Maurin** [a]

† These authors contributed equally

* *E-Mail: guillaume.maurin1@umontpellier.fr*

[a]ICGM, Univ. Montpellier, CNRS, ENSCM, F-34095 Montpellier, France
[b]Research Group for Nanocatalyst (RGN) and Convergent Center for Chemical Process (CCP), Korea Research Institute of Chemical Technology (KRICT), Gajeong-ro 141, Yuseong-gu, Daejeon 34114, South Korea.
[c]Centre National d'Etudes Spatiales, DSO/AQ/LE, 18 Avenue Edouard Belin, 31401 Toulouse, Cedex 09, France

DOI: 10.0000/xxxxxxxxxx

Contents

1. Computational details

1.1. Force field parameters for D4. D4 was modelled as a semi-flexible molecule with an all atom atomistic model. All intramolecular bonds, angles, dihedrals, and cross terms parameters for methyl groups were taken from the consistent-valence force field (CVFF).[S1]

Harmonic Bond

$$U = \frac{1}{2}p_0(r - p_1)^2 \qquad [S1]$$

where p_0/κ_B in units K/Å^2, p_1 in Å.

Table S1: D4 bonding potential parameters.

Pseudo atom	Type of bond	p_0/κ_B (K/Å^2)	p_1 (Å)
Si-O	RIGID_BOND	-	-
Si-C	HARMONIC_BOND	286248.126	1.809
C3-H	HARMONIC_BOND	409668.576	1.105

Harmonic Bend

$$U = \frac{1}{2}p_0(\theta_{\text{ijk}} - p_1)^2 \qquad [S2]$$

where p_0/κ_B in units K/rad^2, p_1 in degree.

Table S2: D4 bending potential parameters.

Pseudo atom	Type of angle	p_0/κ_B (K/rad^2)	p_1 (°)
Si-C-H	HARMONIC_BEND	41614.223	112.3
C-Si-C	HARMONIC_BEND	53400.911	113.5
C-Si-O	HARMONIC_BEND	53040.094	117.3
H-C-H	HARMONIC_BEND	47507.567	106.4

CVFF Dihedral

$$U = p_0(1 + cos(p_1\phi_{\text{ijk}} - p_2))^2 \qquad [S3]$$

where p_0/κ_B in units K, p_2 in degree.

Table S3: D4 dihedral potential parameters.

Pseudo atom	Type of torsion	p_0/κ_B (K)	p_1 (multiplicity)	p_2 (°)
H-C-Si-C	CVFF_DIHEDRAL	240.545	3	0
H-C-Si-O	CVFF_DIHEDRAL	-60.136	3	0
C-Si-O-Si	CVFF_DIHEDRAL	240.545	3	0

CFF Bond Bond Cross

$$U = p_0(r - p_1)(r\prime - p_2) \qquad [S4]$$

where p_0/κ_B in units K/Å^2, p_1 and p_2 in Å

Table S4: D4 cross-term bonding potential parameters.

Pseudo atom	Type of bond-bond	p_0/κ_B (K/Å^2)	p_1 (Å)	p_2 (Å)
Si-C-H	CFF_BOND_BOND_CROSS	14312.406	0	0
C-Si-C	CFF_BOND_BOND_CROSS	7336.612	0	0
C-Si-O	CFF_BOND_BOND_CROSS	25257.188	0	0

CFF Bond Bend Cross

$$U = (\theta - p_0)[p_1(r - p_2) + p_3(r\prime - p_4)] \quad \text{[S5]}$$

where p_0 in degrees, p_1 and p_3 in units K/Å/rad, p_1 and p_2 in Å.

Table S5: D4 cross-term bonding-bending potential parameters.

Pseudo atom	Type of bond-angle	po (°)	p_1 (K/Å/rad)	p_2 (Å)	p_3 (K/Å/rad)	p_4 (Å)
Si-C-H	CFF_BOND_BEND_CROSS	0	14733.359	0	9742.06	0
C-Si-C	CFF_BOND_BEND_CROSS	0	781.770	0	0	0
C-Si-O	CFF_BOND_BEND_CROSS	0	11425.871	0	27061.27	0

D4 LJ parameters and charges

The electronic potential (ESP) derived partial charges of D4 were computed by density functional theory (DFT) calculations with PBE (Perdew-Burke-Ernzerhof) functional[S2] and DNP (double numeric plus polarization) basis set[S3], using DMol^3 module[S4] in Materials Studio[S5] (Table S6).

Table S6: Charges and Lennard-Jones parameters for all atoms of D4.

Pseudo atom	Charge (e$^-$)	ϵ/κ_B (K)	σ (Å)
Si	1.321	202.429	3.826
O	-0.763	30.213	3.118
C	-0.889	52.873	3.431
H	0.2032	22.156	2.571

1.2. Screening dataset. 1710 non-disordered MOFs with pore limiting diameters $>$ 6 Å were screened from CoRE-MOF database, to which 29 well-known MOFs were added with proven stability and high porosity, including the MOF-74 isoreticular series[S6], Cr-soc-MOF-1[S7], UiO-68 (UiO for University of Oslo), MOF-808,[S8] and a several structures originating from Dresden University of Technology (DUT) and Material of Institute Lavoisier (MIL). This additional list is given in Table S7.

The combined dataset of 1739 MOFs show a broad range of geometric and textural features: PLDs (6.0–71.5 Å), N_2 accessible SA (320–6770 $m^2\,g^{-1}$), density (0.13–2.22 $g\,cm^{-3}$), ϕ (0.42–0.94) and PVs (0.23–7.46 $cm^3\,g^{-1}$).

Table S7: Details of the 29 MOFs added to the COREMOF database.

MOFs	Reference	MOFs	Reference
RAVWAO	S6	DUT-5	S9
RAVWES	S6	DUT-51-Zr	S10
RAVWIW	S6	DUT-67-Zr	S11
RAVWOC	S6	MIL-68(Al)	S12
RAVWUI	S6	Cr-soc-MOF-1	S7
RAVXAP	S6	MIP[4]-177	S13
RAVXET	S6	MIP-200	S14
RAVXIX	S6	Zr-IPA[5]	S15
MIL-125	S8	Ni-BPM[6]	S16
MOF-808-acetate	S8	Ni-BPP[7]	S16
MOF-808-formate	S8	Ni-TPM[8]	S16
NU[1]-1000	S8	Ni-TPP[9]	S16
UiO[2]-68	S8	Ni-MOF-74	S16
Zr6-AzoBDC[3]	S8	PCN[10]-224(Ni)	S17

[1]NU: Northwestern University; [2]UiO: University of Oslo;
[3]AzoBDC: azobenzenedicarboxylate;
[4]MIP: material of the Institute of Porous Materials from Paris;
[5]IPA: isophatale; [6]BPM: biphenyl-meta;
[7]BPP: biphenyl-para; [8]TPM: triphenyl-meta;
[9]TPP: triphenyl-para; [10]PCN: Porous coordination network;

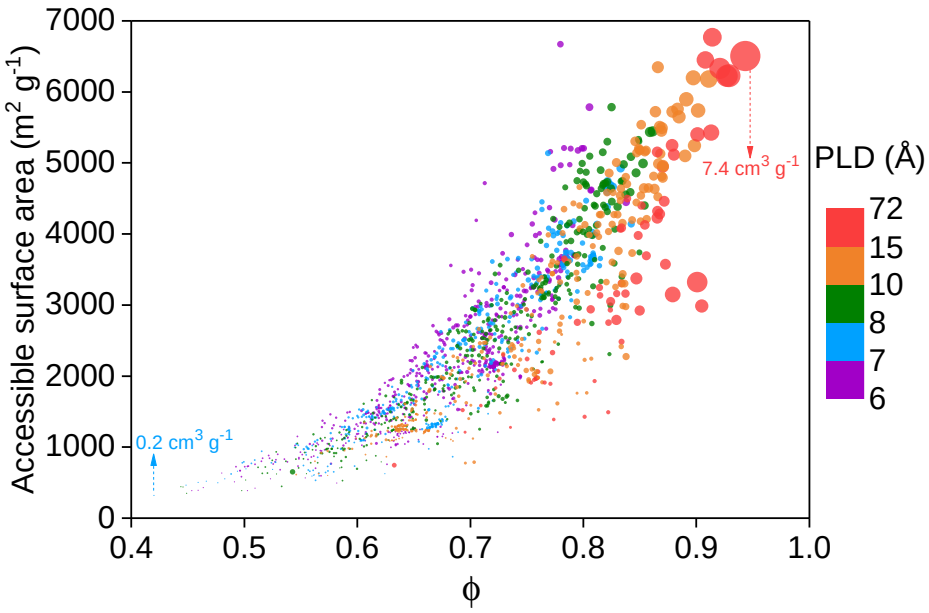

Fig. S1: Overview of the diversity of the MOF database with PLD $>$ 6 Å in terms of void fractions, accessible surface areas and PLDs. Data points are color coded by PLDs of MOFs. Pore volumes of all structures are represented by size.

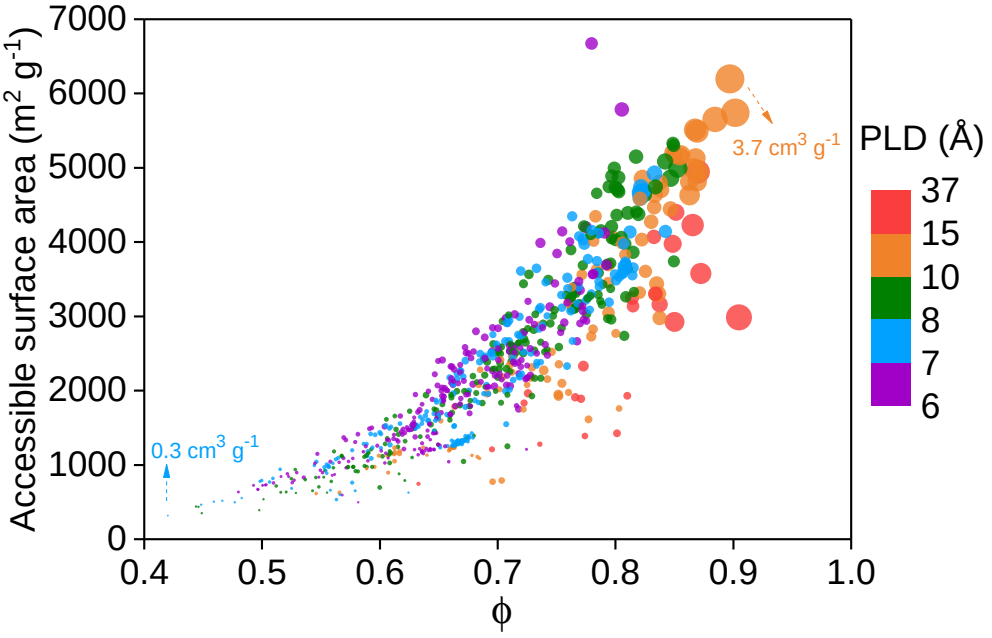

Fig. S2: Overview of the diversity of the hydrophobic MOFs database in terms of void fraction and accessible surface areas. Data points are color coded by PLDs of MOFs. Pore volumes of all structures are represented by size.

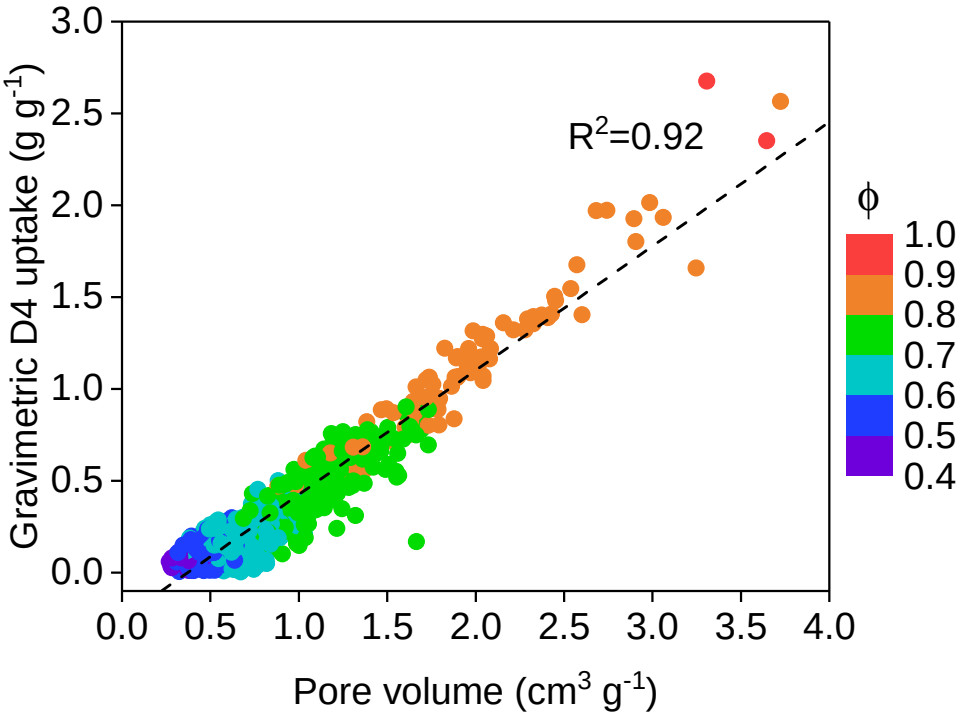

Fig. S3: The relation of gravimetric D4 uptake of the 811 hydrophobic MOFs (g g^{-1}) and their pore volumes (cm^3 g^{-1}), color coded by void fraction of the MOFs.

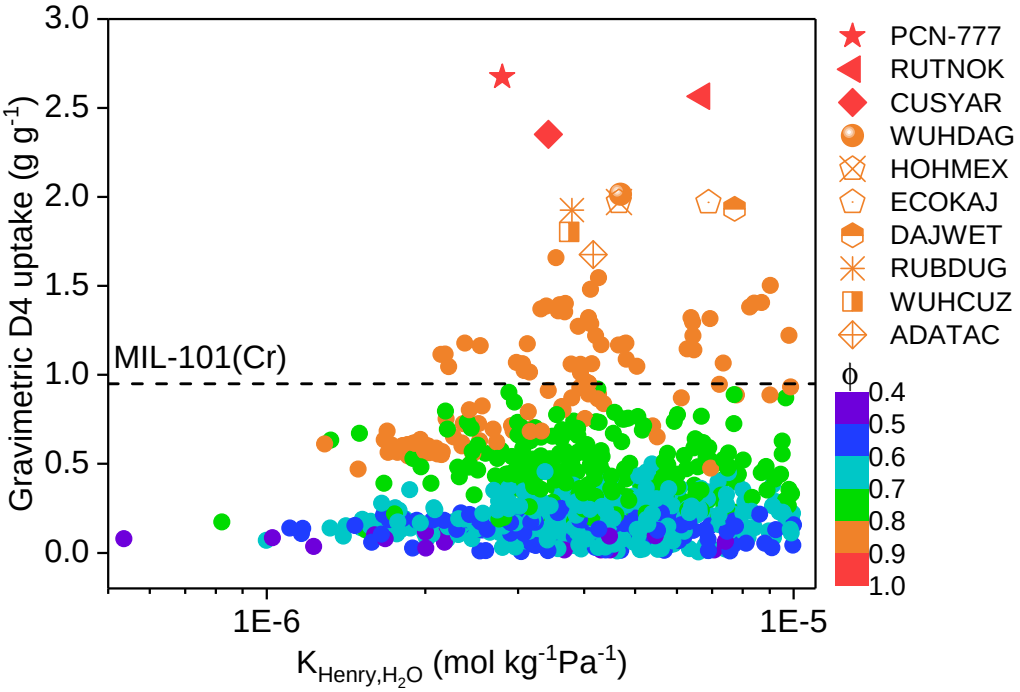

Fig. S4: Predicted D4 uptake performance at 298 K for the hydrophobic MOFs database plotted as a function of their computed Henry constant for water, color coded by void fraction, ϕ. Top performing 10 candidates are represented by different symbols in the legend to the right.

Table S8: Structural details of the top promising 10 hydrophobic materials which exhibit the highest D4 uptake.

MOF	Details
FOTNIN (PCN-777) 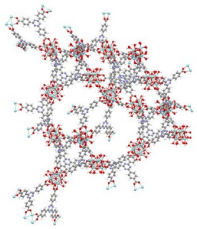	**Organic ligand:** 4,4',4'-s-triazine-2,4,6-triyl-tribenoic acid **Metal site:** Zr **PLD:** 28.36 Å **SA:** 2990 $m^2\,g^{-1}$ **Density:** 0.27 $g\,cm^{-3}$ **PV:** 3.31 $cm^3\,g^{-1}$ ϕ: 0.90 **Gravimetric D4 uptake:** 2.68 $g\,g^{-1}$ **Volumetric D4 uptake:** 0.72 $g\,cm^{-3}$
RUTNOK (IRMOF-76) 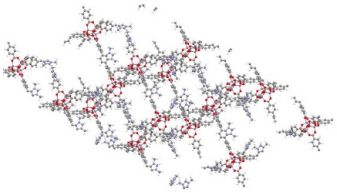	**Organic ligand:** 4,7-bis(4-carboxylphenyl)-1,3-dimethylbenzimidazium-tetrafluoroborate **Metal site:** Zn **PLD:** 14.65 Å **SA:** 6200 $m^2\,g^{-1}$ **Density:** 0.24 $g\,cm^{-3}$ **PV:** 3.72 $cm^3\,g^{-1}$ ϕ: 0.90 **Gravimetric D4 uptake:** 2.57 $g\,g^{-1}$ **Volumetric D4 uptake:** 0.62 $g\,cm^{-3}$
CUSYAR (MOF-210) 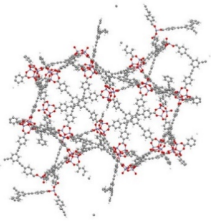	**Organic ligand:** biphenyl-4,4'-dicarboxylate **Metal site:** Zn **PLD:** 12.18 Å **SA:** 5700 $m^2\,g^{-1}$ **Density:** 0.25 $g\,cm^{-3}$ **PV:** 3.65 $cm^3\,g^{-1}$ ϕ: 0.90 **Gravimetric D4 uptake:** 2.35 $g\,g^{-1}$ **Volumetric D4 uptake:** 0.59 $g\,cm^{-3}$
WUHDAG (NU-1104) 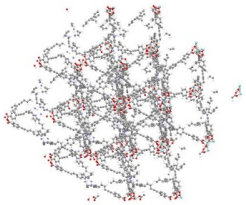	**Organic ligand:** meso-tetrakis-(4-((phenyl)ethynyl)benzoate) porphyrin **Metal site:** Zr **PLD:** 10.50 Å **SA:** 5500 $m^2\,g^{-1}$ **Density:** 0.29 $g\,cm^{-3}$ **PV:** 2.99 $cm^3\,g^{-1}$ ϕ: 0.87 **Gravimetric D4 uptake:** 2.01 $g\,g^{-1}$ **Volumetric D4 uptake:** 0.58 $g\,cm^{-3}$
HOHMEX 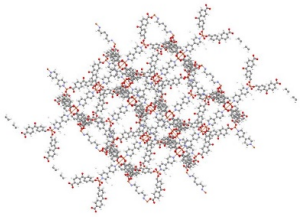	**Organic ligand:** 4,4'-carbonyldibenzoato - (μ2-4,4'-bipyridine) **Metal site:** Cu **PLD:** 14.89 Å **SA:** 5000 $m^2\,g^{-1}$ **Density:** 0.32 $g\,cm^{-3}$ **PV:** 2.74 $cm^3\,g^{-1}$ ϕ: 0.87 **Gravimetric D4 uptake:** 1.97 $g\,g^{-1}$ **Volumetric D4 uptake:** 0.63 $g\,cm^{-3}$
ECOKAJ 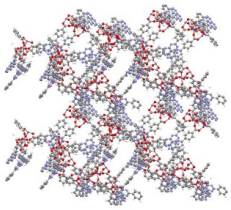	**Organic ligand:** s-heptazine tribenzoate **Metal site:** Zn **PLD:** 17.58 Å **SA:** 3600 $m^2\,g^{-1}$ **Density:** 0.33 $g\,cm^{-3}$ **PV:** 2.68 $cm^3\,g^{-1}$ ϕ: 0.87 **Gravimetric D4 uptake:** 1.97 $g\,g^{-1}$ **Volumetric D4 uptake:** 0.65 $g\,cm^{-3}$

DAJWET

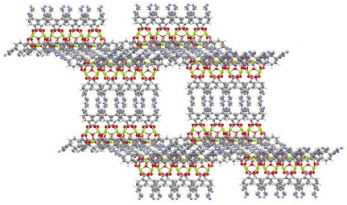

Organic ligand: tetrakis (4-carboxylatophenyl) porphyrin
Metal site: Mg
PLD: 26.59 Å
SA: 5000 $m^2\,g^{-1}$
Density: 0.28 $g\,cm^{-3}$
PV: 3.06 $cm^3\,g^{-1}$
ϕ: 0.87
Gravimetric D4 uptake: 1.93 $g\,g^{-1}$
Volumetric D4 uptake: 0.54 $g\,cm^{-3}$

RUBDUP

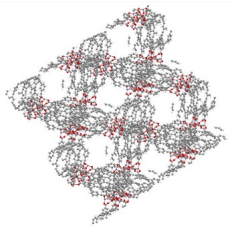

Organic ligand: phenylene ethynylene macrocycle
Metal site: Zn
PLD: 19.25 Å
SA: 4200 $m^2\,g^{-1}$
Density: 0.30 $g\,cm^{-3}$
PV: 2.90 $cm^3\,g^{-1}$
ϕ: 0.87
Gravimetric D4 uptake: 1.93 $g\,g^{-1}$
Volumetric D4 uptake: 0.58 $g\,cm^{-3}$

WUHCUZ (NU-1103)

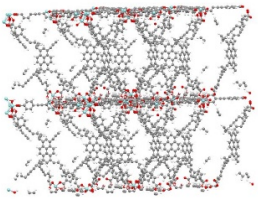

Organic ligand:
4,4‘,4‘‘,4‘‘‘-((pyrene-1,3,6,8 tetrayltetrakis(benzene-4,1-diyl)) tetrakis(ethyne-2,1 diyl))tetrabenzoate
Metal site: Zr
PLD: 12.21 Å
SA: 5500 $m^2\,g^{-1}$
Density: 0.30 $g\,cm^{-3}$
PV: 2.91 $cm^3\,g^{-1}$
ϕ: 0.87
Gravimetric D4 uptake: 1.80 $g\,g^{-1}$
Volumetric D4 uptake: 0.54 $g\,cm^{-3}$

ADATAC

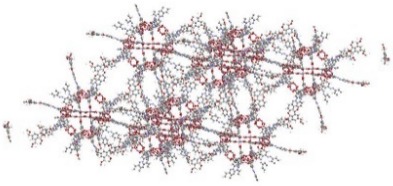

Organic ligand:
5,5‘,5‘‘-(4,4‘,4‘‘-[1,3,5-phenyltris(methoxy)] tris-phenylazo) tris-isophthalic acid
Metal site: Zn
PLD: 10.28 Å
SA: 5130 $m^2\,g^{-1}$
Density: 0.34 $g\,cm^{-3}$
PV: 2.57 $cm^3\,g^{-1}$
ϕ: 0.87
Gravimetric D4 uptake: 1.68 $g\,g^{-1}$
Volumetric D4 uptake: 0.57 $g\,cm^{-3}$

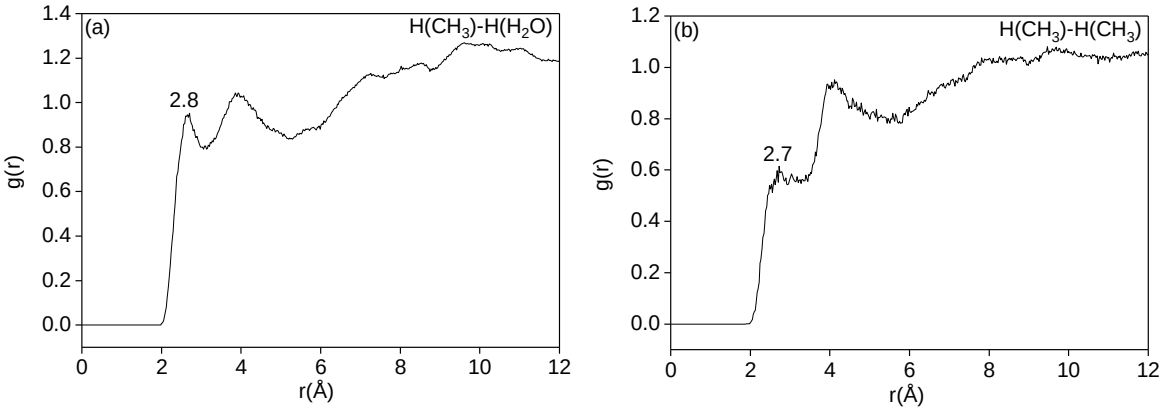

Fig. S5: All-atom averaged radial distribution functions between (a) H atom from CH_3 group of D4 molecules and H atom from coordinated water of the framework at 10% total loading and (b) H atom from CH_3 groups of D4 at 100% loading.

1.3. Radial distribution functions for D4-PCN-777.

2. MOF samples

2.1. MIL-101(Cr). The benchmark MIL-101(Cr) sample was taken from a previous work[S18], with all textural characteristics as stated in reference.

2.2. DUT-4. DUT-4 was purchased from Materials Center (TU Dresden, Germany).

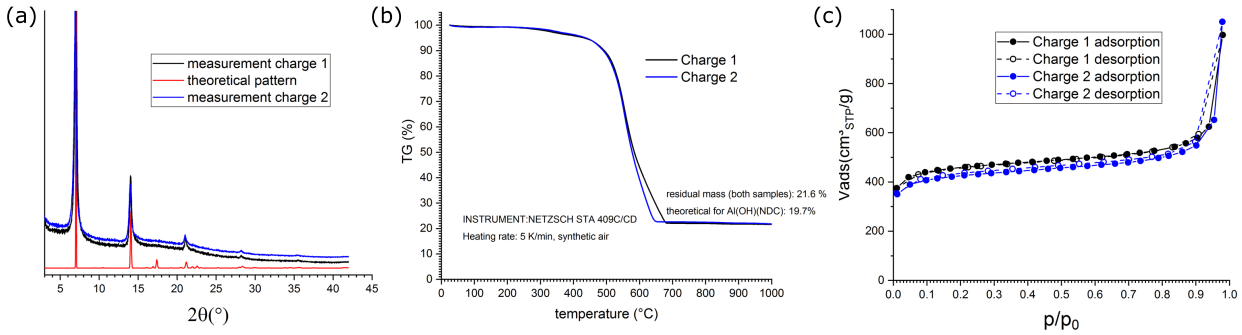

Fig. S6: Characterization of the DUT-4 sample, in duplicates as black and blue: (a) PXRD, alongside simulated pattern in red (b) TGA curves and (c) N_2 physisorption isotherms at 77 K.

2.3. PCN-777. Synthesis

Procedure and activation KRICT

Characterisation

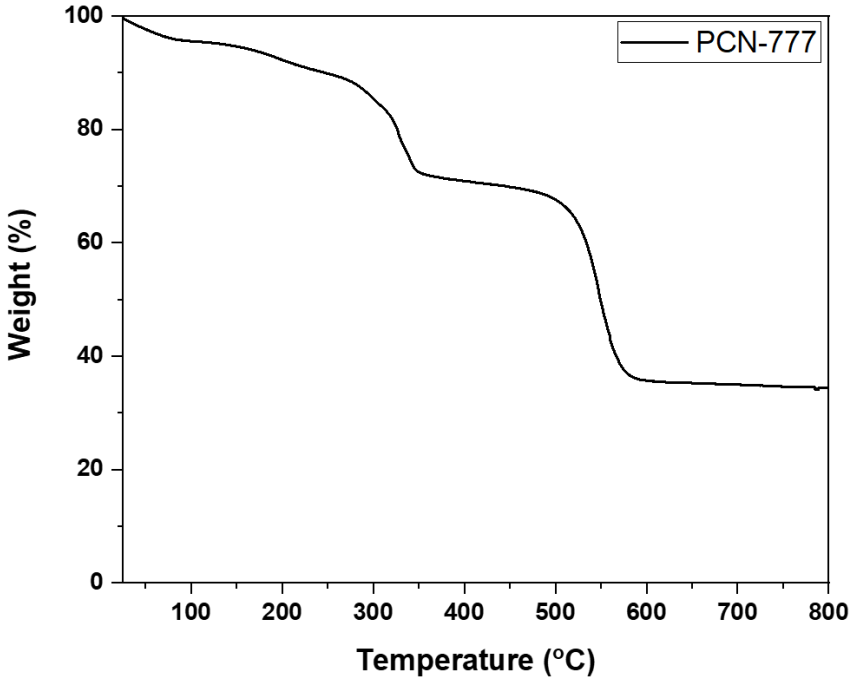

Fig. S7: Thermogravimetric curve recorded on as-synthesised PCN-777.

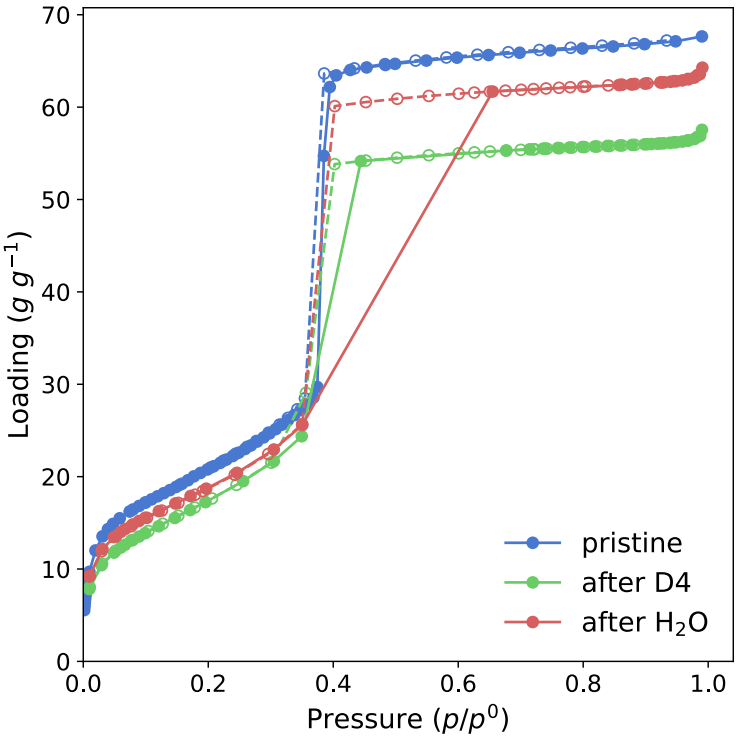

Fig. S8: Nitrogen sorption isotherms at 77 K for the pristine PCN-777, alongside those measured on samples after D4 and water sorption.

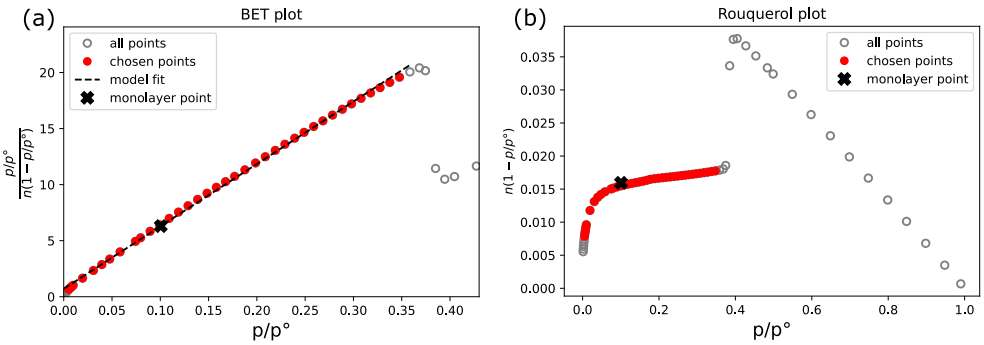

Fig. S9: BET and Rouquerol plots displaying selection of applicable isotherm points for the pristine PCN-777 isotherm.

3. D4 sorption experiments

3.1. D4 benchmarking with known MOFs. Isotherms were recorded on benchmark materials MIL-101(Cr) and DUT-4 using the same methodology detailed in the main manuscript.

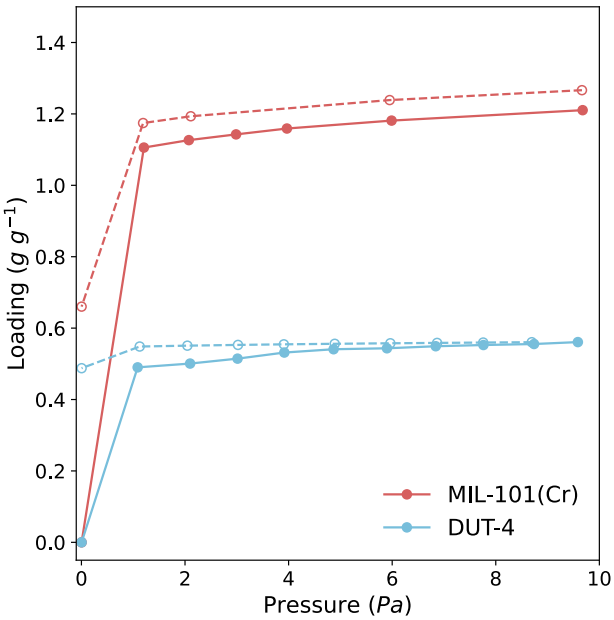

Fig. S10: D4 isotherms recorded on samples of MIL-101(Cr) (red) and DUT-4 (blue), used to validate our computational methodology for predicting total D4 capacity. Note the different desorption behavior (open symbols) of the two materials under secondary vacuum: partial desorption for MIL-101(Cr) and no desorption for DUT-4.

3.2. Isosteric heat of sorption of D4. A further isotherm was recorded at 313 K (40 °C) to allow for the calculation of the isosteric heat of adsorption through the Clausius-Clapeyron equation, as depicted in Fig. S11.

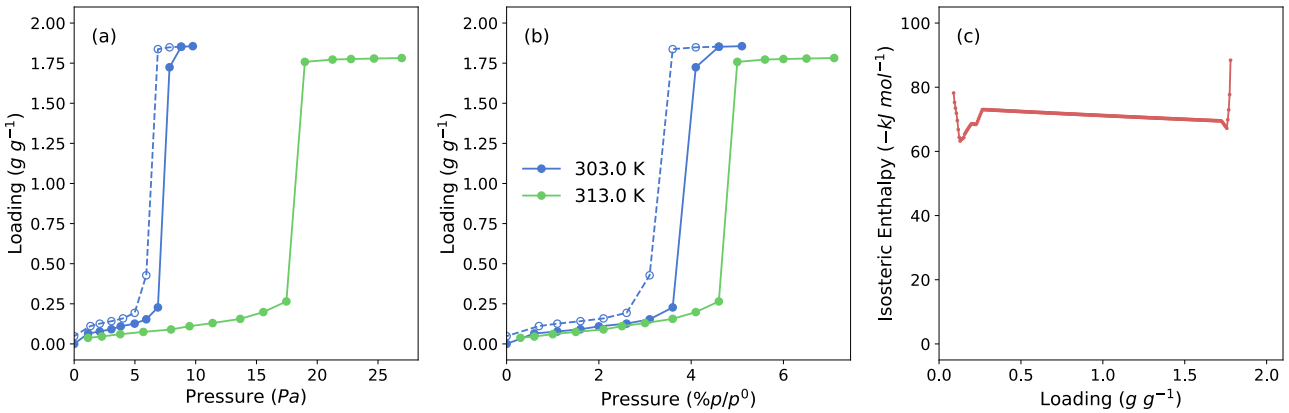

Fig. S11: D4 sorption isotherms on PCN-777 recorded at 303 K (blue) and at 313 K (green) in an absolute (a) and relative (b) pressure scale. (c) The calculated isosteric heat of adsorption as a function of D4 uptake.

References

(S1) Dauber-Osguthorpe, P.; Roberts, V.A.; Osguthorpe, D.J.; Wolff, J.; Genest, M.; and Hagler, A.T. "Structure and energetics of ligand binding to proteins: Escherichia coli dihydrofolate Reductase-Trimethoprim, a Drug-Receptor system." *Proteins: Struct, Funct, Bioinf*, 1988. **4**(1):31–47

(S2) Perdew, J.P.; Burke, K.; and Ernzerhof, M. "Generalized Gradient Approximation Made Simple." *Physical Review Letters*, 1996. **77**(18):3865–3868. doi:10.1103/PhysRevLett.77.3865

(S3) Hehre, W.J.; Ditchfield, R.; and Pople, J.A. "Self-consistent molecular orbital methods. XII. Further extensions of gaussian-type basis sets for use in molecular orbital studies of organic molecules." *J Chem Phys*, 1972. **56**(5):2257–2261

(S4) Delley, B. "An All-electron numerical method for solving the local density functional for polyatomic molecules." *J Chem Phys*, 1990. **92**(1):508–517

(S5) Accelrys. "Materials Studio." Accelrys Software Inc., 2001

(S6) Gulcay, E. and Erucar, I. "Biocompatible MOFs for storage and separation of O2: A molecular simulation study." *Ind Eng Chem Res*, 2019. **58**(8):3225–3237

(S7) Nandi, S.; Aggarwal, H.; Wahiduzzaman, M.; Belmabkhout, Y.; Maurin, G.; Eddaoudi, M.; and Devautour-Vinot, S. "Revisiting the water sorption isotherm of MOF using electrical measurements." *Chem Commun*, 2019. **55**(88):13251–13254

(S8) Soares, C.V.; Leitão, A.; and Maurin, G. "Computational evaluation of the chemical warfare agents capture performances of robust MOFs." *Microporous Mesoporous Mater*, 2019. **280**:97–104

(S9) Senkovska, I.; Hoffmann, F.; Fröba, M.; Getzschmann, J.; Böhlmann, W.; and Kaskel, S. "New highly porous aluminium based metal-organic frameworks: Al(OH)(ndc) (ndc=2,6-naphthalene dicarboxylate) and Al(OH)(bpdc) (bpdc=4,4′-biphenyl dicarboxylate)." *Microporous and Mesoporous Materials*, 2009. **122**(1-3):93–98. doi:10.1016/j.micromeso.2009.02.020

(S10) Bon, V.; Senkovskyy, V.; Senkovska, I.; and Kaskel, S. "Zr(iv) and Hf(iv) based metal–organic frameworks with reo-topology." *Chem Commun*, 2012. **48**(67):8407. doi:10.1039/c2cc34246d

(S11) Bon, V.; Senkovska, I.; Baburin, I.A.; and Kaskel, S. "Zr- and Hf-Based Metal–Organic Frameworks: Tracking Down the Polymorphism." *Crystal Growth & Design*, 2013. **13**(3):1231–1237. doi:10.1021/cg301691d

(S12) Yang, Q.; Vaesen, S.; Vishnuvarthan, M.; Ragon, F.; Serre, C.; Vimont, A.; Daturi, M.; De Weireld, G.; and Maurin, G. "Probing the adsorption performance of the hybrid porous MIL-68(Al): A synergic combination of experimental and modelling tools." *Journal of Materials Chemistry*, 2012. **22**(20):10210. doi:10.1039/c2jm15609a

(S13) Wang, S.; Kitao, T.; Guillou, N.; Wahiduzzaman, M.; Martineau-Corcos, C.; Nouar, F.; Tissot, A.; Binet, L.; Ramsahye, N.; Devautour-Vinot, S.; Kitagawa, S.; Seki, S.; Tsutsui, Y.; Briois, V.; Steunou, N.; Maurin, G.; Uemura, T.; and Serre, C. "A phase transformable ultrastable titanium-carboxylate framework for photoconduction." *Nature Communications*, 2018. **9**(1). doi:10.1038/s41467-018-04034-w

(S14) Wang, S.; Lee, J.S.; Wahiduzzaman, M.; Park, J.; Muschi, M.; Martineau-Corcos, C.; Tissot, A.; Cho, K.H.; Marrot, J.; Shepard, W.; Maurin, G.; Chang, J.S.; and Serre, C. "A robust large-pore zirconium carboxylate metal–organic framework for energy-efficient water-sorption-driven refrigeration." *Nat Energy*, 2018. **3**(11):985–993. doi:10.1038/s41560-018-0261-6

(S15) Wang, S.; Chen, L.; Wahiduzzaman, M.; Tissot, A.; Zhou, L.; Ibarra, I.A.; Gutiérrez-Alejandre, A.; Lee, J.S.; Chang, J.S.; Liu, Z.; Marrot, J.; Shepard, W.; Maurin, G.; Xu, Q.; and Serre, C. "A Mesoporous Zirconium-Isophthalate Multifunctional Platform." *Matter*, 2020. p. S2590238520305634. doi:10.1016/j.matt.2020.10.009

(S16) Zheng, J.; Barpaga, D.; Trump, B.A.; Shetty, M.; Fan, Y.; Bhattacharya, P.; Jenks, J.J.; Su, C.Y.; Brown, C.M.; Maurin, G.; McGrail, B.P.; and Motkuri, R.K. "Molecular Insight into Fluorocarbon Adsorption in Pore Expanded Metal–Organic Framework Analogs." *J Am Chem Soc*, 2020. **142**(6):3002–3012. doi:10.1021/jacs.9b11963

(S17) Feng, D.; Chung, W.C.; Wei, Z.; Gu, Z.Y.; Jiang, H.L.; Chen, Y.P.; Darensbourg, D.J.; and Zhou, H.C. "Construction of Ultrastable Porphyrin Zr Metal–Organic Frameworks through Linker Elimination." *J Am Chem Soc*, 2013. **135**(45):17105–17110. doi:10.1021/ja408084j

(S18) Pillai, R.S.; Yoon, J.W.; Lee, S.J.; Hwang, Y.K.; Bae, Y.S.; Chang, J.S.; and Maurin, G. "N $_2$ Capture Performances of the Hybrid Porous MIL-101(Cr): From Prediction toward Experimental Testing." *J Phys Chem C*, 2017. **121**(40):22130–22138. doi:10.1021/acs.jpcc.7b07029